Journal of Manufacturing Processes 105 (2023) 307–312

Contents lists available at ScienceDirect

Journal of Manufacturing Processes

journal homepage: www.elsevier.com/locate/manpro

A geometric approach to milling stability uncertainty☆

Tony Schmitz

University of Tennessee, Knoxville, United States of America
Oak Ridge National Laboratory, United States of America

ARTICLE INFO

Keywords:
Milling
Stability
Chatter
Uncertainty

ABSTRACT

Deterministic solutions for the milling stability boundary are provided by frequency-domain, time-domain, and semi-discretization methods. While these deterministic solutions are valuable, it is essential to consider the uncertainty in the predicted stability boundary to enable optimum milling parameter selection. Prior efforts have implemented Type A (statistical) uncertainty evaluations. This paper provides a Type B (other means) analysis, where the stability uncertainty is represented by offset boundaries based on user-selected uncertainties in spindle speed and axial depth. The geometric approach is demonstrated for a selected milling system using a frequency-domain stability solution.

1. Introduction

An important consideration for milling parameter selection is chatter, a self-excited vibration that occurs when the axial depth of cut exceeds a limiting value for a selected spindle speed and radial depth of cut. The separation between stable and unstable combinations of spindle speed and axial depth is depicted graphically as a stability map [1]. This map can be generated using frequency-domain, time-domain, or semi-discretization methods, all of which have been verified experimentally [2]. Inputs to these analyses include the tool tip frequency response function (FRF) which represents the vibration response at the free end of the cutting tool, the mechanistic cutting force model coefficients that relate the cutting force components to the instantaneous chip thickness and width, number of cutting teeth, radial depth of cut, and milling direction (up/conventional or down/climb milling). The spindle speed is considered to be the independent variable and the limiting axial depth is calculated as the dependent variable.

While deterministic solutions for the milling stability boundary exist, it is important to consider the effect of uncertainties in the input parameters on the corresponding stability boundary uncertainty [3]. The motivation is inherent uncertainties in the stability algorithm and the inputs. The aleatoric algorithm uncertainties are based on approximations and assumptions in the stability model and assumptions about the model inputs (the description of cutting force by a linear mechanistic force model and its associated coefficients, for example). The epistemic input uncertainties, on the other hand, are based on measurement uncertainty (the complex-valued tool tip FRF, for example). Because the model and inputs are uncertain, the predicted stability boundary is also uncertain. To make the best use of the predicted stability map, it is required that the confidence in the prediction is evaluated. This provides a probabilistic solution and, consequently, a predictive model for milling stability.

In 2005, Kurdi et al. first evaluated the uncertainty in milling performance prediction, including both stability and surface location error (SLE), a part geometry error caused by forced vibrations [4]. They estimated confidence in parameter optimization results based on uncertainty in the milling model input parameters. They applied both Monte Carlo simulation and numerical derivatives of the system eigenvalues to evaluate the uncertainty in axial depth of cut. Duncan et al. reported the addition of confidence intervals to the milling stability limit in 2006 [5]. Uncertainties in the tool tip FRF, cutting force model coefficients, and radial depth of cut, were used to determine the associated uncertainty in the predicted stability limit at each spindle speed; see Fig. 1 for an example, where it is observed that experimental results do not exactly agree with the (mean) predicted stability limit, but the uncertainty intervals capture the physical behavior. Specifically, spindle speed-axial depth pairs below the uncertain interval are predicted to be stable, pairs above are predicted to be unstable (chatter), and those

E-mail address: tony.schmitz@utk.edu.

https://doi.org/10.1016/j.jmapro.2023.09.032
Received 26 February 2023; Received in revised form 3 May 2023; Accepted 10 September 2023
Available online 25 September 2023

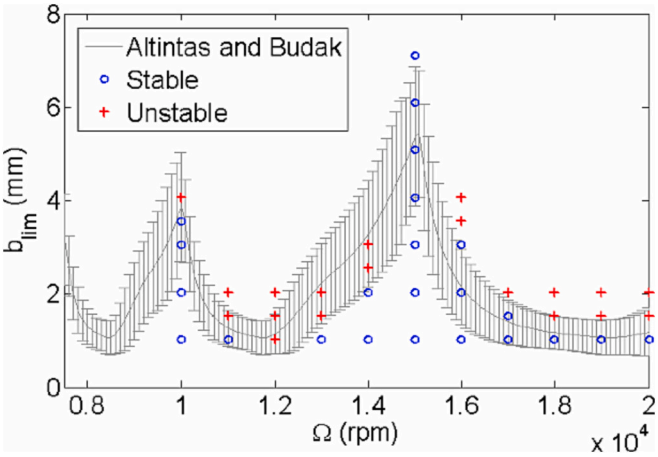

Fig. 1. Example stability boundary with spindle speed-dependent, 95 % confidence intervals. The vertical axis is the limiting axial depth of cut, b_{lim}, and the horizontal axis is spindle speed, Ω. Experimental results are also included [5].

within the uncertain interval may be stable or unstable. In related work, Duncan predicted the tool tip FRF using receptance coupling substructure analysis (RCSA) and propagated uncertainty in the predicted FRF through frequency-domain stability models [6].

Lee and Donmez studied the effect of changes in dynamics of the tool-holder-spindle system on stability limit uncertainty [7]. Kurdi et al. determined the variability in stability boundary and surface location error using Latin Hypercube sampling. They described the experimental procedures used to estimate the model parameters and included the effect of correlation between parameters [8,9]. Sims et al. applied fuzzy arithmetic techniques to frequency domain and time-finite element stability analyses [10]. Zhang et al. maximized material removal rate and minimized surface location error using an optimization formulation, where the upper bound of surface location error and lower bound of the stability boundary were adopted as the optimization object and the constraint condition, respectively [11]. Graham et al. used the edge theorem and the zero-exclusion condition to develop a robust chatter stability model [12]. Graham et al. extended this work to include a time domain approach based on Lyapunov stability theory and subjected to linear matrix inequality conditions [13]. Cao and Li developed a robust chatter stability model for micro-milling based on a frequency-domain stability milling model, where the edge theorem and the zero-exclusion condition were again implemented [14].

Bayesian (probabilistic) methods have been applied to milling stability modeling by multiple authors. Bayesian inference was first applied by Karandikar et al. in 2014 [15]. A Bayesian approach was implemented that used a random walk strategy for establishing a stability model. The stability boundary was modeled using random walks and the probability of the random walk being the true stability limit was updated using experiments. Karandikar et al. also described automated identification of the milling stability boundary using Bayesian machine learning and experiments [16]. The user's initial beliefs about milling stability, or prior, were updated using experiments to calculate the posterior, a modified probabilistic description of the milling stability limit with reduced uncertainty based on the new information. Karandikar et al. later proposed a Bayesian learning approach for stability boundary and optimal parameter identification in milling that did not require knowledge of the tool tip dynamics or cutting force model coefficients [17]. Li et al. estimated posterior milling parameter distributions using a Bayesian inference framework based on an ensemble Markov Chain Monte Carlo algorithm [18]. Cornelius et al. described a physics-guided Bayesian framework for identifying the milling stability boundary and system parameters through iterative testing [19]. Prior uncertainties for the parameters were identified without physical testing of the actual milling system. Those uncertainties were propagated to the stability uncertainty using Monte Carlo simulation; this established the prior. The uncertainties were then updated based on new information acquired from cutting tests to calculate the posterior. Chen et al. also proposed a physics-informed Bayesian inference framework for milling stability which leveraged experimental data to infer the distribution of model parameters [20]. The likelihood function was based on Floquet theory in this study. Schmitz et al. described a milling stability identification approach that simultaneously considered physics-based models for the tool tip frequency response functions and stability predictions; the binary result from a milling test; chatter frequency when an unstable result was obtained; and user risk tolerance [21]. The algorithm applied probabilistic Bayesian machine learning with adaptive, parallelized Markov Chain Monte Carlo sampling to update the probability of stability with each milling test.

Other methods have also been applied to evaluate the milling stability boundary uncertainty. Huang et al. applied the dimension reduction method to compute statistical moments of the limit state function. Saddle point approximation was employed to estimate the probability density function, cumulative distribution function, and dynamic stability reliability [22]. Hadju et al. determined robust stability boundaries based on the concept of stability radius and structured singular values using an extended multi-frequency stability solution [23]. Liu et al. introduced a time-varying reliability analysis to predict chatter stability by considering the cutting force model coefficients to be both random and time-varying variables [24]. Löser et al. calculated a robust stability limit using a computationally efficient approximation of a multi-frequency stability solution [25]. Deng et al. established a chatter reliability model, where the tool tip FRF modal parameters were defined as random variables. The second-order fourth-moment method was applied; the limiting axial cutting depth was substituted by an explicit expression obtained using a neural network [26]. Hadju et al. presented a robust stability analysis based on a pseudo-spectral approach to incorporate uncertainties in the cutting force model coefficients and modal parameters used to describe the tool tip FRF. Operational modal analysis was conducted at different spindle speeds to identify the natural frequencies and damping ratios of the dominant vibration modes using impact testing [27]. Deng et al. applied a generalized regression neural network to obtain the stability boundary at different positions within a machine tool's work volume [28].

In related work, Junior et al. described the relationship between the pre-setter tool extension length and diameter measurements, the tool tip FRF, and milling stability [29]. The RCSA technique was used within a Monte Carlo simulation to establish the tool point FRF uncertainty as a function of the tool extension length and diameter uncertainties. The distribution in the tool point FRF was then propagated to uncertainty in the milling stability limit. Bhattacharyya et al. derived empirical models for cutting forces and propagated uncertainties using: 1) a first-order Taylor series expansion and a root sum of squares method to analytically determine the expanded uncertainty in force predictions; and 2) Monte Carlo simulation to numerically determine the statistical distributions and uncertainties [30]. The literature contributions are summarized chronologically in Table 1.

2. Uncertainty evaluation background

As stated in NIST Technical Note 1297 [31], 'the result of a measurement is only an approximation or estimate of the value of the specific quantify in question, that is, the measurand, and thus the result is complete only when accompanied by a quantitative statement of its uncertainty'. The inclusion of a defensible uncertainty statement enables the user to determine his/her confidence in the measurement and its usefulness in decision making. This concept can be extended to simulation results based on measured input quantities. Again, the user requires some indication of the reliability of the analysis output to gage its usefulness. Guidelines for evaluating the uncertainty in measurement

Table 1
Chronological literature summary for milling uncertainty evaluation studies.

First author	Year	Topic
Kurdi, M.H.	2005	Used Monte Carlo simulation and numerical derivatives of the system eigenvalues to evaluate the uncertainty in axial depth of cut
Duncan, G. S.	2006	Used Monte Carlo simulation to propagate parameter input uncertainty through analytical milling stability models
Duncan, G. S.	2006	Used Monte Carlo simulation to propagate uncertainty in tool tip FRF predicted using RCSA through analytical milling stability models
Lee, K.J.	2007	Studied effect of changes in dynamics of the tool-holder-spindle system during the milling operation on stability limit uncertainty
Kurdi, M.H.	2009	Evaluated variability in stability boundary and surface location error using Latin Hypercube sampling
Sims, N.D.	2010	Applied fuzzy arithmetic techniques to uncertainty in frequency domain and time-finite element stability analyses
Zhang, X.	2012	Maximized material removal rate and minimized surface location error using an optimization formulation
Graham, E.	2013	Used the edge theorem and the zero-exclusion condition to develop a robust chatter stability model
Graham, E.	2014	Described time domain approach based on Lyapunov stability theory and subjected to linear matrix inequality conditions
Karandikar, J.	2014	Modeled the stability boundary using random walks in a Bayesian framework
Cao, Z.	2015	Used the edge theorem and the zero-exclusion condition to develop a robust chatter stability model for micro-milling
Huang, X.	2016	Applied dimension reduction method and saddle point approximation to estimate reliability of the dynamic stability
Hajdu, D.	2017	Determined robust stability boundaries based on the concept of the stability radius and structured singular values
Liu, Y.	2017	Introduced a time-varying reliability analysis with variable cutting force model coefficients
Löser, M.	2018	Calculated a robust stability map using an approximation of the multi-frequency stability solution
Junior, M.V.	2018	Described the relationship between the pre-setter tool extension length and diameter measurements, the tool tip FRF, and stability
Deng, C.	2020	Established a chatter reliability model using the second-order fourth-moment method and a neural network
Hadju, D.	2020	Presented a robust stability analysis based on a pseudo-spectral approach that incorporated uncertainties in the cutting force model coefficients and modal parameters
Bhattacharyya, A.	2021	Derived empirical models for cutting forces and propagated uncertainties using a first-order Taylor series expansion and Monte Carlo simulation
Cornelius, A.	2021	Described a physics-guided Bayesian framework for identifying the milling stability boundary and system parameters through iterative testing
Chen, G.	2021	Proposed physics-informed Bayesian inference framework for milling stability
Deng, C.	2022	Applied a generalized regression neural network to obtain the position-dependent stability boundaries
Schmitz, T.	2022	Applied Bayesian machine learning to physics-based prior with adaptive, parallelized Markov Chain Monte Carlo sampling

results are described in [31–34], for example. Often the measurand is not observed directly, but is expressed as a mathematical function of multiple input quantities. In this case, the fundamental steps in uncertainty estimation are to define the measurand, identify the input uncertainty contributors and their distributions, and propagate the uncertainties through the measurand using either analytical (Taylor series expansion) or sampling (e.g., Monte Carlo or Latin hypercube) approaches. As noted in [31], the 'uncertainty of the result of a measurement generally consists of several components which may be grouped into two categories according to the method used to estimate their numerical values: A. those which are evaluated by statistical methods, B. those which are evaluated by other means.'

In previous milling stability evaluation, Type A analyses were followed where distributions of the model input parameters, including the tool tip FRF (or its representation by modal parameters) and cutting force coefficients, were propagated through the stability analysis to evaluate stability boundary uncertainty using a statistical evaluation of the boundary distribution (e.g., mean and standard deviation). Generally, the cutting force coefficients tend to shift the stability boundary up and down (in axial depth), while the tool tip FRF (or modal parameters) tend to shift the stability boundary not only up and down, but also left and right (in spindle speed). This couples the spindle speed-axial depth boundary coordinates to the inputs, but their relationship is defined by the selected stability analysis and a direct connection between the input uncertainties and stability boundary uncertainty is not straightforward to identify. This has motivated the Type A analyses in the literature.

Because milling stability analyses consider spindle speed to be the independent variable, the uncertainty in axial depth has been reported as spindle speed dependent. In this paper, a Type B approach is selected where uncertainty in the stability boundary location in the (spindle speed, axial depth), or (Ω, b), domain is based on user-selected uncertainties (or offsets, o) in both the spindle speed and axial depth directions. A stability map is then constructed using a geometric approach to show the mean stability limit and uncertainty intervals based on the user's beliefs and risk preference (averse, neutral, or seeking). For the purposes of this paper, the mean stability limit represents the deterministic solution based on the mean inputs.

3. Geometric approach

As shown in Fig. 2, the uncertainty is accommodated using an offset (dashed line) of the mean stability boundary (solid line) by a Euclidean distance, d; see Eq. 1. In Fig. 2, (Ω_1, b_1) and (Ω_2, b_2) are adjacent points on the mean stability boundary and (Ω_{1a}, b_{1a}) is a point on the offset boundary which corresponds to (Ω_1, b_1). The perpendicular distance, d, is calculated from: 1) the user-selected boundary offsets in spindle speed, o_Ω, and axial depth, o_b; and 2) the angle, θ, of the vector between points 1 and 1a which depends on the local slope of the stability boundary. See Fig. 3, which shows θ and its relationship to d, and Eq. 2, where the absolute value in axial depth difference is required because the mean stability boundary slope can be positive or negative.

$$d = \sqrt{(o_b cos\theta)^2 + (o_\Omega sin\theta)^2} \tag{1}$$

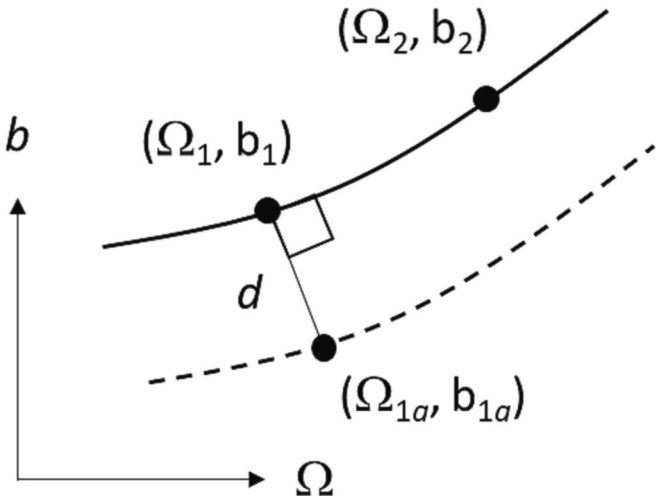

Fig. 2. Mean stability boundary (solid line) and offset boundary (dashed line) using the distance, d.

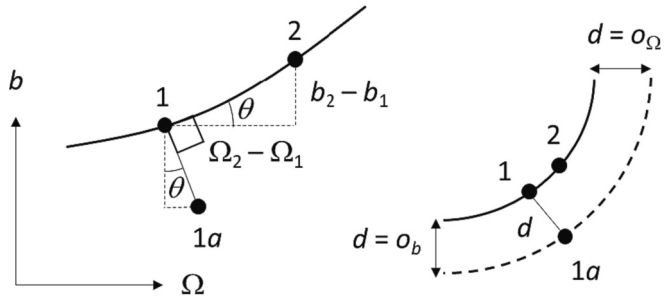

Fig. 3. Calculation of d using θ as shown in Eq. 2. The variation in d from o_b (when $\theta = 0$) to o_Ω (when $\theta = 90$ deg) is displayed on the right.

$$\theta = tan^{-1}\frac{|b_2 - b_1|}{\Omega_2 - \Omega_1} \tag{2}$$

Given d, two steps are followed to determine the coordinates of point $1a$, (Ω_{1a}, b_{1a}), on the offset boundary. The first step is to apply the dot product to perpendicular vectors $\boldsymbol{A}$ and $\boldsymbol{B}$, where $\boldsymbol{A}$ is the vector from point 1 to point 2 on the mean stability boundary and $\boldsymbol{B}$ is the vector from point 1 and point $1a$ on the offset stability boundary. The vectors are shown in Fig. 4.

The dot product of vectors $\boldsymbol{A}$ and $\boldsymbol{B}$ is given by Eq. 3, where $A_x = \Omega_2 - \Omega_1$, $B_x = \Omega_{1a} - \Omega_1$, $A_y = b_2 - b_1$, and $B_y = b_{1a} - b_1$.

$$cos90 = 0 = \frac{A \bullet B}{|A||B|} = \frac{A_x B_x + A_y B_y}{|A||B|} \tag{3}$$

Substitution of A_x, B_x, A_y, and B_y in Eq. 3 gives Eq. 4.

$$0 = (\Omega_2 - \Omega_1)(\Omega_{1a} - \Omega_1) + (b_2 - b_1)(b_{1a} - b_1) \tag{4}$$

The second step is to apply the Pythagorean theorem to Fig. 5. This provides a relationship between d and the unknown coordinates of point $1a$, (Ω_{1a}, b_{1a}). The result is provided in Eq. 5.

$$d^2 = (b_1 - b_{1a})^2 + (\Omega_{1a} - \Omega_1)^2 \tag{5}$$

Eq. 4 is rewritten to solve for Ω_{1a}.

$$\Omega_{1a} = \Omega_1 + \frac{(b_2 - b_1)}{(\Omega_2 - \Omega_1)} b_{1a} + \frac{(b_2 - b_1)}{(\Omega_2 - \Omega_1)} b_1 \tag{6}$$

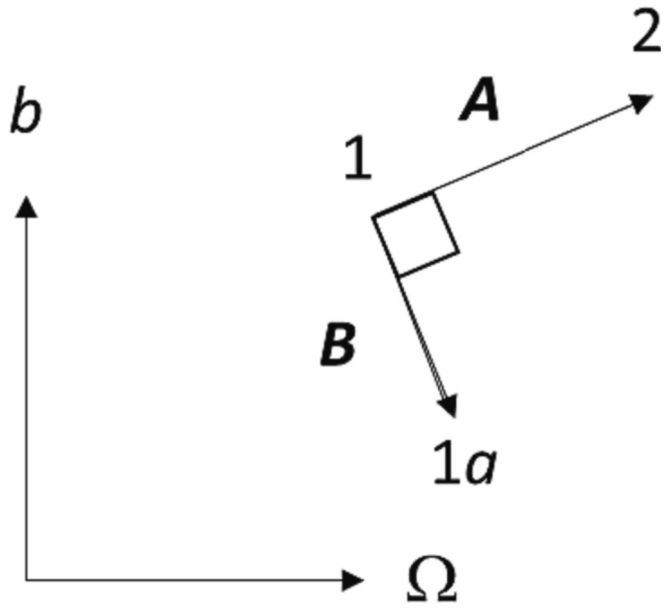

Fig. 4. Perpendicular vectors $\boldsymbol{A}$ and $\boldsymbol{B}$ used to calculate the dot product.

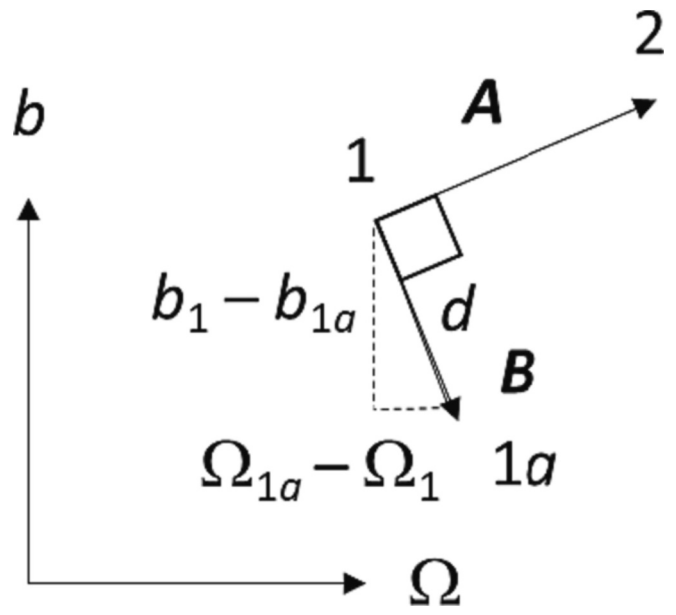

Fig. 5. Application of Pythagorean theorem to provide relationship between d and the coordinates of point $1a$ on the offset boundary.

Eq. 6 is substituted into Eq. 5.

$$d^2 = (b_1 - b_{1a})^2 + \left(\frac{-(b_2 - b_1)}{(\Omega_2 - \Omega_1)} b_{1a} + \frac{(b_2 - b_1)}{(\Omega_2 - \Omega_1)} b_1\right)^2 \tag{7}$$

Eq. 7 is expanded to solve for b_{1a}, where $A = b_1$, $B = \frac{-(b_2 - b_1)}{(\Omega_2 - \Omega_1)}$, and $C = \frac{(b_2 - b_1)}{(\Omega_2 - \Omega_1)} b_1$.

$$d^2 = (A - b_{1a})^2 + (Bb_{1a} + C)^2 = A^2 - 2Ab_{1a} + b_{1a}^2 + B^2 b_{1a}^2 + 2BCb_{1a} + C^2 \tag{8}$$

Eq. 8 is rearranged into quadratic equation format in Eq. 9, where $D = 1 + B^2$, $E = -2A + 2BC$, and $F = A^2 + C^2 - d^2$. The quadratic formula is applied to Eq. 9 to give the solutions for b_{1a} in Eq. 10.

$$Db_{1a}^2 + Eb_{1a} + F = 0 \tag{9}$$

$$b_{1a} = \frac{-E \pm \sqrt{E^2 - 4DF}}{2D} \tag{10}$$

The two solutions from Eq. 10 represent the upper (maximum b_{1a} value) and lower (minimum b_{1a} value) offset boundaries for the uncertain stability map. Finally, the corresponding spindle speed for either value is calculated using Eq. 11.

$$\Omega_{1a} = \Omega_1 + Bb_{1a} + C \tag{11}$$

The solution procedure given by Eqs. 1–11 is applied sequentially to each point along the mean (deterministic) stability boundary to identify the corresponding points on the upper and lower offset boundaries.

4. Numerical example

To demonstrate the geometric approach, an example milling system is specified and offset boundaries are generated for user-selected spindle speed, o_Ω, and axial depth, o_b, offset values. The frequency-domain stability solution presented by Altintas and Budak [35] is implemented to calculate the mean stability boundary. The milling system parameters are:

- 20 % radial immersion down milling
- 4 teeth

- single degree of freedom, symmetric tool tip FRFs represented by a stiffness of 3×10^6 N/m, a viscous damping ratio of 3 %, and a natural frequency of 750 Hz
- a cutting force model with a specific cutting force of 750 N/mm^2 and a force angle of 68 deg. (aluminum alloy).

The offsets for this numerical example are $o_\Omega = 100$ rpm and $o_b = 0.2$ mm = 200 μm. The selection of these two offset values is user dependent. The nature of a Type B analysis is that "other means" are used to establish the uncertainty. A user with a higher risk tolerance would choose smaller offsets to select parameters nearer the mean boundary, while one with a lower risk tolerance (risk averse) would choose larger offsets to avoid obtaining unstable (chatter) cutting conditions. The 0.2 mm value selected for the analysis is what the author would consider to be a small axial depth offset. The actual values would depend on the application. If parameters were being selected for finish machining a high value forging where significant value is already embedded in the part, for example, larger offset values may be chosen.

Fig. 6 displays the mean stability limit together with the upper and lower offset boundaries. The corresponding θ and d values for the upper (Figs. 7 and 8) and lower (Figs. 9 and 10) offsets are also provided (blue circles), together with the associated offset boundaries (green dots). It is seen that the θ and d values are invariant (for the selected milling system). Choosing the minimum or maximum value from Eq. 10 defines the offset boundary coordinates.

The reader will note that Figs. 6-10 have units of micrometers for axial depth (right vertical axis). Because spindle speeds are typically in thousands of rpm, the selection of micrometers for axial depth provides approximately the same scaling for both variables and avoids the requirement for normalizing variables prior to solving Eqs. 1–11. If desired, the axial depth coordinates may be converted back to the traditional unit of millimeters for plotting purposes.

Close observation of Figs. 7-10 demonstrates the relationship between d and θ represented conceptually in Fig. 3. At spindle speeds of 5660 rpm and 11,298 rpm, where local maxima in axial depth occur, θ approaches 90 deg. in Figs. 7 and 9 (left vertical axis). The corresponding d values approach $o_\Omega = 100$ rpm in Figs. 8 and 10 (left vertical axis). At a spindle speed of 6960 rpm, where a local minimum in axial depth occurs, θ approaches 0 deg. in Figs. 7 and 9. The corresponding d value approaches $o_b = 200$ μm in Figs. 8 and 10.

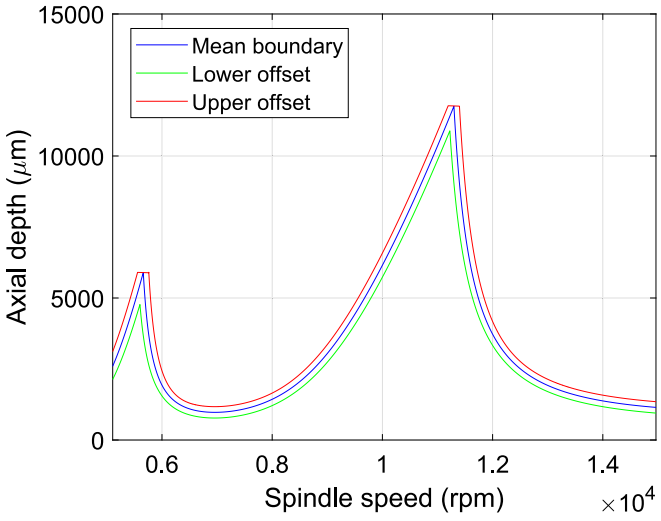

Fig. 6. Mean stability limit with upper and lower offset boundaries with $o_\Omega = 100$ rpm and $o_b = 0.2$ mm = 200 μm.

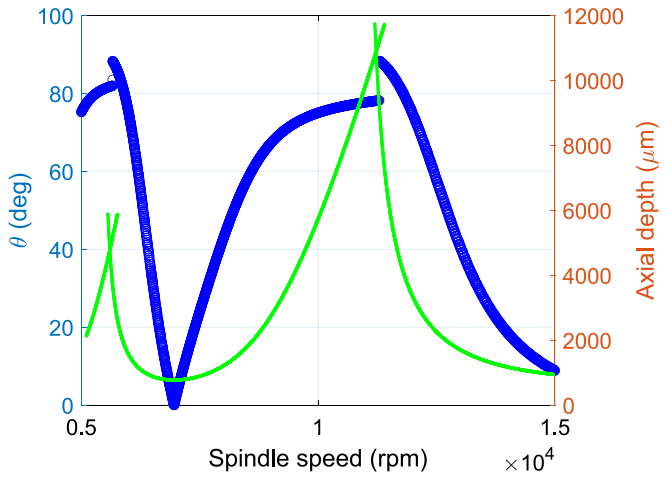

Fig. 7. Lower offset boundary (green dots, right vertical axis) and θ values (blue circles, left vertical axis). (For interpretation of the references to colour in this figure legend, the reader is referred to the web version of this article.)

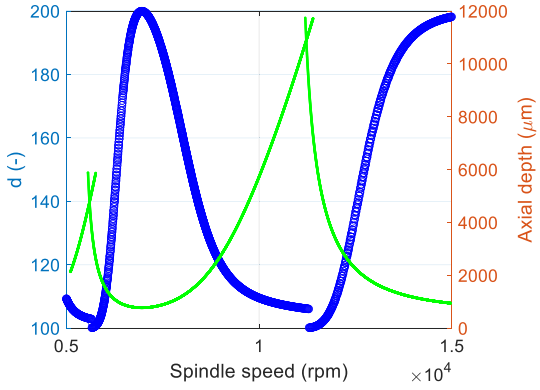

Fig. 8. Lower offset boundary (green dots, right vertical axis) and d values (blue circles, left vertical axis). (For interpretation of the references to colour in this figure legend, the reader is referred to the web version of this article.)

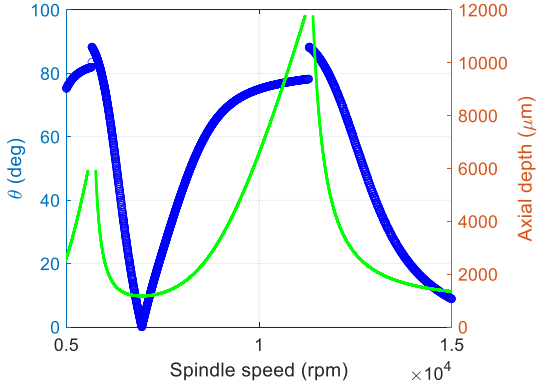

Fig. 9. Upper offset boundary (green dots, right vertical axis) and θ values (blue circles, left vertical axis). (For interpretation of the references to colour in this figure legend, the reader is referred to the web version of this article.)

5. Conclusions

This paper described a Type B approach to milling stability boundary uncertainty evaluation. In the new geometric approach, stability boundary location uncertainty in the (Ω, b) domain was based on user-selected uncertainties in both the spindle speed, o_Ω, and axial depth, o_b,

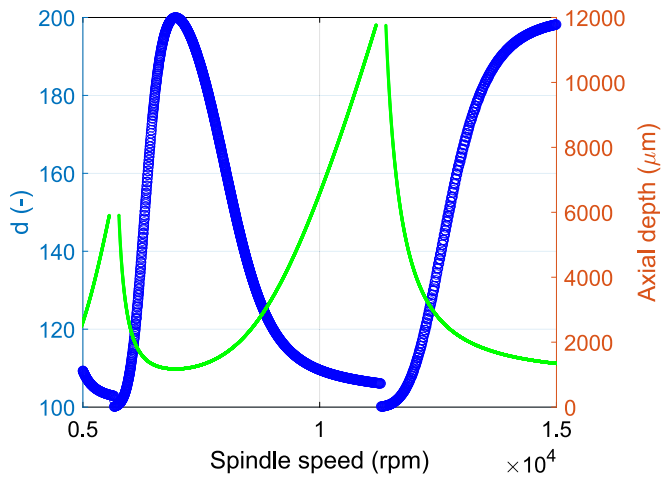

Fig. 10. Upper offset boundary (green dots, right vertical axis) and d values (blue circles, left vertical axis). (For interpretation of the references to colour in this figure legend, the reader is referred to the web version of this article.)

directions. A stability map was then constructed with the mean stability limit and uncertainty intervals based on (o_Ω, o_b), which represent the user's beliefs and risk preference (averse, neutral, or seeking). These uncertainty intervals were graphically represented as upper and lower boundaries offset by a Euclidean distance based on the local slope of the mean stability boundary and the user-selected uncertainties.

The offset boundaries were determined using a two-step approach. The first step was to calculate the dot product of perpendicular vectors defined using adjacent points on the mean stability boundary and a pair of points connecting the mean stability boundary and offset boundary. The second step was to apply the Pythagorean theorem to this perpendicular vector geometry. The result was a system of two nonlinear equations in two unknowns: the two coordinates of point $1a$, (Ω_{1a}, b_{1a}), on the offset boundary which correspond to point 1 on the mean stability boundary. These two steps were repeated for each point on the mean stability boundary. Points on the upper and lower boundaries were identified from the two roots of a quadratic equation. Numerical results were provided to demonstrate the approach.

The outcome of this research is an alternate milling stability uncertainty analysis that enables the user to directly specify his/her preferences for a Euclidean distance between the mean and offset stability boundaries. Future work will include the extension of this analysis to SLE [36] and tool length-dependent stability surfaces [37].

Declaration of competing interest

The author declares that he has no known competing financial interests or personal relationships that could have appeared to influence the work reported in this paper.

Acknowledgements

This research was supported by the DOE Office of Energy Efficiency and Renewable Energy (EERE), Energy and Transportation Science Division, and used resources at the Manufacturing Demonstration Facility, a DOE EERE User Facility at Oak Ridge National Laboratory.

References

[1] Schmitz T, Smith KS. Machining dynamics: Frequency response to improved productivity. 2nd ed. New York, NY: Springer; 2019.
[2] Altintas Y, Stepan G, Budak E, Schmitz T, Kilic ZM. Chatter stability of machining operations. J Manuf Sci Eng 2020;142(11).
[3] Schmitz TL, Karandikar J, Ho Kim N, Abbas A. Uncertainty in machining: workshop summary and contributions. J Manuf Sci Eng 2011;133(5).
[4] Kurdi, M.H., Schmitz, T.L., Haftka, R.T. and Mann, B.P., 2005, January. A numerical study of uncertainty in stability and surface location error in high-speed milling. In ASME international mechanical engineering congress and exposition (Vol. 42231, pp. 387-395).
[5] Duncan GS, Kurdi MH, Schmitz TL, Snyder JP. Uncertainty propagation for selected analytical milling stability limit analyses. Milwaukee, WI, Society of Manufacturing Engineers (SME): Transactions of NAMRI/SME; 2006. p. 17–24.
[6] Duncan GS. Milling dynamics prediction and uncertainty analysis using receptance coupling substructure analysis. Dissertation: University of Florida; 2006.
[7] Lee, K.J. and Donmez, M.A., 2007, January. Repeatability analysis on the tool point dynamics for investigation on uncertainty in milling stability. In ASME international mechanical engineering congress and exposition (Vol. 42975, pp. 477-483).
[8] Kurdi MH, Schmitz TL, Haftka RT, Mann BP. Milling optimisation of removal rate and accuracy with uncertainty: part 1: parameter selection. Int J Mater Product Technol 2009;35(1–2):3–25.
[9] Kurdi MH, Schmitz TL, Haftka RT, Mann BP. Milling optimisation of removal rate and accuracy with uncertainty: part 2: parameter variation. Int J Mater Product Technol 2009;35(1–2):26–46.
[10] Sims ND, Manson G, Mann B. Fuzzy stability analysis of regenerative chatter in milling. J Sound Vib 2010;329(8):1025–41.
[11] Zhang X, Zhu L, Zhang D, Ding H, Xiong Y. Numerical robust optimization of spindle speed for milling process with uncertainties. Int J Mach Tool Manuf 2012; 61:9–19.
[12] Graham E, Mehrpouya M, Park SS. Robust prediction of chatter stability in milling based on the analytical chatter stability. J Manufact Proc 2013;15(4):508–17.
[13] Graham E, Mehrpouya M, Nagamune R, Park SS. Robust prediction of chatter stability in micro milling comparing edge theorem and LMI. CIRP J Manufact Sci Technol 2014;7(1):29–39.
[14] Cao Z, Li H. Investigation of machining stability in micro milling considering the parameter uncertainty. Adv Mech Eng 2015;7(3). p.1687814015575982.
[15] Karandikar J, Traverso M, Abbas A, Schmitz T. Bayesian inference for milling stability using a random walk approach. J Manuf Sci Eng 2014;136(3).
[16] Karandikar J, Honeycutt A, Smith S, Schmitz T. Milling stability identification using Bayesian machine learning. Procedia CIRP 2020;93:1423–8.
[17] Karandikar J, Honeycutt A, Schmitz T, Smith S. Stability boundary and optimal operating parameter identification in milling using Bayesian learning. J Manufact Proc 2020;56:1252–62.
[18] Li K, He S, Liu H, Mao X, Li B, Luo B. Bayesian uncertainty quantification and propagation for prediction of milling stability lobe. Mech Syst Signal Proc 2020; 138:106532.
[19] Cornelius A, Karandikar J, Gomez M, Schmitz T. A Bayesian framework for milling stability prediction and reverse parameter identification. Procedia Manufacturing 2021;53:760–72.
[20] Chen G, Li Y, Liu X, Yang B. Physics-informed Bayesian inference for milling stability analysis. Int J Mach Tool Manuf 2021;167:103767.
[21] Schmitz T, Cornelius A, Karandikar J, Tyler C, Smith S. Receptance coupling substructure analysis and chatter frequency-informed machine learning for milling stability. CIRP Annals 2022;71(1):321–4.
[22] Huang X, Zhang Y, Lv C. Probabilistic analysis of dynamic stability for milling process. Nonlinear Dynamics 2016;86:2105–14.
[23] Hajdu D, Insperger T, Bachrathy D, Stepan G. Prediction of robust stability boundaries for milling operations with extended multi-frequency solution and structured singular values. J Manufact Proc 2017;30:281–9.
[24] Liu Y, Wang ZY, Liu K, Zhang YM. Chatter stability prediction in milling using time-varying uncertainties. Int J Adv Manufact Technol 2017;89:2627–36.
[25] Löser M, Otto A, Ihlenfeldt S, Radons G. Chatter prediction for uncertain parameters. Adv Manufact 2018;6:319–33.
[26] Deng C, Miao J, Ma Y, Wei B, Feng Y. Reliability analysis of chatter stability for milling process system with uncertainties based on neural network and fourth moment method. Int J Prod Res 2020;58(9):2732–50.
[27] Hajdu D, Borgioli F, Michiels W, Insperger T, Stepan G. Robust stability of milling operations based on pseudospectral approach. Int J Mach Tool Manuf 2020;149: 103516.
[28] Deng C, Shu J, Ma Y, Lu S, Zhao Y, Miao J. Multi-objective modelling and optimal parameter selection of a multi-pass milling process considering uncertain milling stability constraint. Int J Adv Manufact Technol 2022;120(9–10):6225–40.
[29] Junior MV, Baptista EA, Araki L, Smith S, Schmitz T. The role of tool presetting in milling stability uncertainty. Procedia Manufacturing 2018;26:164–72.
[30] Bhattacharyya A, Schueller JK, Mann BP, Schmitz TL, Gomez M. Uncertainty propagation through an empirical model of cutting forces in end milling. J Manuf Sci Eng 2021;143(7).
[31] Taylor, B.N. and C.E. Kuyatt, 1994, Guidelines for evaluating and expressing the uncertainty of NIST measurement results. NIST technical note 1297 1994 edition.
[32] International Standards Organization (ISO), 1993, Guide to the Expression of Uncertainty in Measurement (Corrected and Reprinted 1995).
[33] American National Standards Institute. ANSI/NCSL Z540–2-1997. US: Guide to the Expression of Uncertainty in Measurement; 1997.
[34] Bevington PR, Robinson DK. Data reduction and error analysis for the physical sciences. 2nd ed. Boston, MA: WCB/McGraw-Hill; 1992.
[35] Altintaş Y, Budak E. Analytical prediction of stability lobes in milling. CIRP Annals 1995;44(1):357–62.
[36] Honeycutt A, Schmitz TL. Surface location error and surface roughness for period-n milling bifurcations. J Manuf Sci Eng 2017;139(6).
[37] Schmitz TL, Burns TJ, Ziegert JC, Dutterer B, Winfough WR. Tool length-dependent stability surfaces. Mach Sci Technol 2004;8(3):377–97.